



HAL
open science

Ternary antimonides $\text{Ln 2Pd}_9\text{Sb}_3$ ($\text{Ln} = \text{La, Ce, Nd, Pr, and Sm}$): Crystal, electronic structure, and magnetic properties

O. Zhak, T. Zdorov, V. Levytsky, V. Babizhetskyy, C. Zheng, O. Isnard

► To cite this version:

O. Zhak, T. Zdorov, V. Levytsky, V. Babizhetskyy, C. Zheng, et al.. Ternary antimonides $\text{Ln 2Pd}_9\text{Sb}_3$ ($\text{Ln} = \text{La, Ce, Nd, Pr, and Sm}$): Crystal, electronic structure, and magnetic properties. *Journal of Alloys and Compounds*, 2020, 815, pp.152428. 10.1016/j.jallcom.2019.152428 . hal-03488872

HAL Id: hal-03488872

<https://hal.science/hal-03488872>

Submitted on 20 Jul 2022

HAL is a multi-disciplinary open access archive for the deposit and dissemination of scientific research documents, whether they are published or not. The documents may come from teaching and research institutions in France or abroad, or from public or private research centers.

L'archive ouverte pluridisciplinaire **HAL**, est destinée au dépôt et à la diffusion de documents scientifiques de niveau recherche, publiés ou non, émanant des établissements d'enseignement et de recherche français ou étrangers, des laboratoires publics ou privés.



Distributed under a Creative Commons Attribution - NonCommercial 4.0 International License

**TERNARY ANTIMONIDES $Ln_2Pd_9Sb_3$ ($Ln = La, Ce, Nd, Pr, \text{ and } Sm$): CRYSTAL,
ELECTRONIC STRUCTURE, AND MAGNETIC PROPERTIES**

O. Zhak^a, T. Zdorov^a, V. Levytsky^a, V. Babizhetskyy^a, C. Zheng^b, O. Isnard^{c,*}

^a*Faculty of Chemistry, Ivan Franko National University of Lviv, Kyryla i Mefodiya Str. 6, UA-
79005 Lviv, Ukraine*

^b*Department of Chemistry and Biochemistry, Northern Illinois University, DeKalb, IL 60115, USA*

^c*Institut Néel, University Grenoble Alpes and CNRS, 25 Rue des Martyrs, BP 166, Cedex 9,
Grenoble, F-38042, France*

* Corresponding author: Prof. O. ISNARD
Tel : +33 (0)4 76 88 11 46, Fax: +33 (0)4 76 88 10 00
E-mail address: olivier.isnard@neel.cnrs.fr

Abstract

A series of new ternary antimonides $Ln_2Pd_9Sb_3$ ($Ln = La, Pr, Nd, Sm$) was synthesized from pure constituents. The crystal structure of all compounds was determined by X-ray powder diffraction. These compounds are isotypic with the $Ce_2Pd_9Sb_3$ structure (anti-type to the ternary gallide $Y_2Co_3Ga_9$, space group $Cmcm$): $a = 13.7772(6)$, $b = 8.0642(3)$, $c = 9.3967(4)$ Å for $La_2Pd_9Sb_3$; $a = 13.7392(6)$, $b = 8.0146(3)$, $c = 9.3215(4)$ Å for $Pr_2Pd_9Sb_3$; $a = 13.7208(5)$, $b = 7.9983(3)$, $c = 9.3016(3)$ Å for $Nd_2Pd_9Sb_3$; $a = 13.6957(7)$, $b = 7.9686(4)$, $c = 9.2700(5)$ Å for $Sm_2Pd_9Sb_3$. The electronic structures of $Ln_2Pd_9Sb_3$ were analyzed using the tight-binding extended Hückel method on cerium representative. The analysis of the magnetic properties shows that the $Ln_2Pd_9Sb_3$ ($Ln = La, Nd, Pr, \text{ and } Sm$) compounds are paramagnetic down to a very low temperature. Curie-Weiss paramagnetic temperature are small and range from between -6 to -1 K. The Sm and Pr containing phases exhibits the largest ordering temperature of 6.8 and 6.2 K, respectively. The Ce containing phase also orders magnetically below 4 K in contrast to the La one (which remains paramagnetic even at 2 K), thus indicating that Ce is carrying an ordered magnetic moment. At 2 K, the magnetization curves of these compounds do not saturate easily even in applied fields up of 10 T.

Keywords: rare-earth intermetallics; crystal structure; X-ray diffraction; electronic structure; magnetic properties.

Introduction

The ternary Ln -Pd-Sb systems, where Ln represents a rare earth metal, have not been investigated systematically earlier. Only the corresponding isothermal section of the solid-state phase diagram of the ternary Er-Pd-Sb system has been constructed [1]. For the other systems, especially with the light rare earth metals, only data about compositions and crystal structures of some ternary compounds are available [2]. It should be mentioned that a number of the ternary rare-earth and palladium antimonides are of great interest because of their physical properties, first of all thermoelectric, e.g. ternary phases $RPdZ$, where $Z = Sb, Bi$ [3]; superconducting such as $LaPd_2Sb_2$ (CaBe₂Ge₂-type structure) and $LaPdSb_2$ (ZrCuSi₂-type structure) [4]; and heavy fermion behavior, for example Ce containing phases $CeTSb_2$ ($T = Ni, Cu, Pd, \text{ and } Ag$) and $CePdX$ ($X = As, Sb$) [5, 6]. The ternary compound $Ce_2Pd_9Sb_3$ with the orthorhombic structure of the anti- $Y_2Co_3Ga_9$ type (space group $Cmcm$) has been reported earlier by [7], but no other isotypic compounds with other rare earths have been obtained. The crystal structure of the ternary cerium and palladium antimonide $Ce_2Pd_9Sb_3$ was determined using X-ray single crystal diffraction data, and atomic arrangement was discussed as the same as in the $Y_2Co_3Ga_9$ type with the interchanged sites of the d -metal and p -elements, forming as a result, the antitype to the $Y_2Co_3Ga_9$ structure [7]. Earlier we reported a new ternary antimonide $La_2Pd_9Sb_3$, which crystallizes with the orthorhombic anti- $Y_2Co_3Ga_9$ type structure [8]. In this paper we present the crystal structures of new light rare earth metal representatives of the $Ce_2Pd_9Sb_3$ type. The ternary antimonides $Ln_2Pd_9Sb_3$ ($Ln = Nd, Pr, \text{ and } Sm$) were synthesized for the first time from the pure elements and investigated in detail in this work. Crystal structure of these compounds was determined by X-ray powder diffraction. No physical properties have been reported on these $Ln_2Pd_9Sb_3$ compounds except some preliminary data on the electrical and paramagnetic behavior of $Ce_2Pd_9Sb_3$ [7]. Here we extend the investigation of the magnetic properties to the $Ln_2Pd_9Sb_3$ compounds with $Ln = La, Ce, Nd, Pr, \text{ and } Sm$ in a wide temperature range from room temperature down to 2 K.

Experimental details

Samples for the investigation have been prepared by arc melting of pre-sintered mixtures of the pure components. Starting materials for the synthesis of the $Ln_2Pd_9Sb_3$ compounds were chips of the rare earth metals (Johnson Matthey, with minimum purity 99.98 wt. % of rare earth element), and palladium and antimony powders (Johnson Matthey, with 99.99 wt. % of purity). Weighed mixtures of the constituents in the 2:9:3 stoichiometric ratios were pressed into pellets. The pellets

were placed into the evacuated fused silica tubes and slowly heated up to 870 K (100 K per 24 hours), kept at this temperature over 240 h, and then cooled down to room temperature by switching off the furnace. The sintered samples were arc-melted under purified argon atmosphere, and finally, the alloys were annealed in the evacuated fused silica tubes at 870 K for 4 weeks, thereafter quenched in cold water without breaking the tubes. The final mass of the annealed samples did not deviate from the initial mass of the unreacted mixtures by more than 2 %.

All samples have been studied by X-ray diffraction. The resulting data were used for phase and structural analysis. The powder diffraction intensity data were collected on an automatic powder diffractometer STOE STADI P: transmission mode; curved germanium (111) monochromator; linear PSD detector; Cu $K\alpha_1$ -radiation; $\lambda = 0.154056$ nm; 2θ -range $6.000 \leq 2\theta \leq 110.625^\circ$, step 0.015° of 2θ , scan time 270 sec/step. The WinCSD software [9] has been used for all calculations including the Rietveld refinement of the crystal structure.

The crystal orbital overlap populations (COOP) were computed using the tight-binding extended Hückel method (EH) [10, 11]. 125 k -points in the irreducible wedge of the Brillouin zone were used in the EH computations. The EH parameters used are (orbital energies in eV with the Slater orbital exponents in parentheses): Ce $6s$ -4.97 (1.799), $6p$ -4.97 (2.20), $5d$ -6.43 (3.90 and 2.10, C_1 0.7765, C_2 0.4586); Pd $5s$ -7.32 (2.19), $5p$ -3.75 (2.152), $4d$ -12.02 (5.983 and 2.613, C_1 0.5535, C_2 0.6701); Sb $5s$ -18.80 (2.323), $5p$ -11.70 (1.999). The spin-polarized densities of states (DOS) were calculated by the WIEN2k package based on the full-potential (linearized) augmented plane-wave + local orbitals method using all default parameters [12]. 1000 k -points were generated and then reduced to the irreducible wedge of the Brillouin zone. [The calculations were carried without the LDA+ \$U\$ approximation.](#)

The magnetic measurements have been undertaken on powder samples in the temperature range from 1.7 to 300 K. The measurements have been made using the extraction method on an experimental set up described elsewhere [13]. Temperature dependence of the magnetization in field-cooling regime as well as isothermal magnetization measurements have been recorded. The isothermal magnetization curves have been performed in magnetic field up to 10 T.

Results and discussion

Crystal structure

During the systematic investigation of the interaction between rare earth metals, palladium and antimony, a number of the ternary $Ln_2Pd_9Sb_3$ compounds, where $Ln = La, Ce, Nd, Pr, \text{ and } Sm$, were synthesized, and atomic parameters in the crystal structures of all obtained $Ln_2Pd_9Sb_3$ antimonides

were refined from X-ray powder diffraction data using the program suite WinCSD. As a starting model, the atomic coordinates in the $Ce_2Pd_9Sb_3$ structure (space group $Cmcm$) published in [7] were used. For all the synthesized $Ln_2Pd_9Sb_3$ compounds the same type of crystal structure was confirmed. The obtained crystal structure data and the details of the structure refinement are listed in Table 1 and Table 2.

Fig. 1 shows the X-ray diffraction patterns of the new antimonides $Pr_2Pd_9Sb_3$, $Nd_2Pd_9Sb_3$, and $Sm_2Pd_9Sb_3$. As one can see, the powder diffraction pattern of these compounds does not show detectable amount of impurities of other phases.

The ternary antimonides $Ln_2Pd_9Sb_3$, where $Ln = La, Pr, Nd, \text{ and } Sm$, are the new members of the series of the isotypic compounds of the $Ce_2Pd_9Sb_3$ type structure (or anti- $Y_2Co_3Ga_9$ type) formed by the light rare earth metals with palladium and antimony. In this structure, the large atoms of the rare earth metals occupy the $8g$ sites, palladium atoms are in four Wyckoff positions $16h, 8g, 8f$ and $4c$, and the antimony atoms occupy two sites $8e$ and $4a$, as a result forming the fully ordered atomic distribution, the same as was determined earlier for the $Ce_2Pd_9Sb_3$ structure. Therefore, in the structure of the $Ln_2Pd_9Sb_3$ antimonides ($Ce_2Pd_9Sb_3$ -type), palladium atoms occupy the crystallographic positions of the gallium atoms whereas antimony atoms occupy the respective positions of the cobalt atoms in the structure of the $Y_2Co_3Ga_9$ type forming the anti-type to the ternary gallide $Y_2Co_3Ga_9$ [14]. At the same time the largest rare earth atoms occupy the position of the yttrium. Peculiarities of the $Ce_2Pd_9Sb_3$ crystal structure were discussed in details earlier in [7].

Projection of the $Nd_2Pd_9Sb_3$ structure onto the xz plane is given in Fig. 2 (a). Coordination polyhedra of the rare earth atoms are distorted hexagonal prisms formed by Pd and Sb atoms with the additional five palladium atoms in the front of the rectangular faces. As such, the coordination number (CN) of the Nd atom is equal to 17. For both antimony atoms Sb1, Sb2, and for the palladium atoms Pd1, Pd2, Pd4, the coordination numbers are equal to 12. The nearest neighbors of the Sb2, Pd2 and Pd4 atoms form the icosahedral coordination. Atom Pd3 is in the center of the 13-vertex polyhedron that can be obtained from the Frank-Kasper 14-vertex [15] prototype by subtracting one. Coordination polyhedra of the Sb1 and Sb2 atoms are formed by all types of Pd and Nd atoms, and completely fill the structure of $Nd_2Pd_9Sb_3$ in the xy plane as shown in Fig. 2 (b). Interatomic distances in the structures of the new antimonides are nearly the same as the respective sums of the metallic radii of the pure components ($r_{La} = 1.870 \text{ \AA}$, $r_{Ce} = 1.825 \text{ \AA}$, $r_{Pr} = 1.820 \text{ \AA}$, $r_{Nd} = 1.814 \text{ \AA}$, $r_{Sm} = 1.802 \text{ \AA}$, $r_{Pd} = 1.376 \text{ \AA}$, $r_{Sb} = 1.41 \text{ \AA}$ [16]) indicating predominantly metallic type of bonding. For example, in the $Nd_2Pd_9Sb_3$ crystal structure maximal contraction of the distances is observed between palladium and antimony atoms: $\delta_{Pd2-Sb1} = 2.577(2) \text{ \AA}$, and $\delta_{Pd4-Sb2} = 2.604(3) \text{ \AA}$, but the largest decrease of interatomic distances does not exceed 7.5 % of the sum of the metallic radii of Pd and Sb. A close Pd-Sb distances indicate a strong interaction between

these two type of atoms, when compared the sum of their covalent radii, 2.68 Å. Such close Pd-Sb distances has also been observed in Ce₃Pd₆Sb₅ [17], Ce₈Pd₂₄Sb, [18], and EuPd₂Sb₂ [19]. A short Pd(2)-Pd(2) bond with a distance of 2.700(5) Å is a little bit smaller than the Pd-Pd distance of 2.751 Å in the palladium metal. The rare earth atoms have one rare earth metal neighbor, forming the pairs. In the crystal structures of Ln₂Pd₉Sb₃, where Ln = La, Pr, Nd, and Sm, the largest distances $\delta_{Ln-Ln} = 4.355(6)$ Å were detected for Pr₂Pd₉Sb₃, indicating a weak interaction between the praseodymium atoms, whereas for larger cerium atoms in the crystal structure of Ce₂Pd₉Sb₃ the $\delta_{Ce-Ce} = 4.292(8)$ Å.

With the aim of the evaluation of the valence state of the rare earth atoms we have analyzed dependence of the lattice parameters versus atomic or ionic size of the rare earth. The variations of the unit cell volume V as a function of the size of the Ln³⁺ ion ($r_{La(III)} = 1.03$ Å, $r_{Ce(III)} = 1.01$ Å, $r_{Pr(III)} = 0.99$ Å, $r_{Nd(III)} = 0.98$ Å, $r_{Sm(III)} = 0.96$ Å, according to Shannon [20]) are shown for the series of the isotopic compounds in Fig. 3. The dependence reflects the effect of lanthanide contraction, and indicates the same valence state (+3) for all the atoms.

Electronic structure

A simple valence electron partitioning of Ln₂Pd₉Sb₃ leads to a valence state of (Ln³⁺)₂(Pd₉)³⁺(Sb³⁻)₃ considering that Sb is most electronegative in Allred-Rochow scale of the three (La: 1.08, Pd: 1.35, Sb: 1.85). This partitioning imposes an oxidation state of +0.33 on each Pd. There will be therefore a small depletion of electrons in the filled 4d¹⁰ subshell. It is well known that even for a filled d¹⁰ subshell, there can be significant d¹⁰-d¹⁰ attractive interaction due to the mixing of the higher s and p orbitals [21]. Because of the electron depletion in the 4d¹⁰ subshell, this interaction will be strengthened. The relatively small Pd-Pd distances in the structure reflect such an increased bonding interaction.

Figure 4 shows the EH COOP curves of three representative bonds calculated for the Ce₂Pd₉Sb₃ compound. In the left panel, all states contribute to Ce-Pd bonding as expected, since Ce³⁺ has an empty 5d subshell. Since the Ce-Pd distance is large, the overlap population integrated to the Fermi level is small at 0.04. In the middle panel, all states below the Fermi level are also of Pd-Sb bonding character, the states centered around -19.5 eV being the Sb 5s and around -12 eV Sb 5p. The integrated overlap population of 0.37 indicates a strong covalent bonding. In the right panel, the states below -12 eV contribute to Pd-Pd bonding, then they become antibonding before return to bonding just below the Fermi level. This is a typical d¹⁰-d¹⁰ attractive interaction feature: Below d⁵ the states are bonding, and from d⁵ to d¹⁰ antibonding. Because of the 4d subshell depletion and the mixing from the s and p states above, there is small bonding character below the Fermi level. The

overall interaction is of bonding character, as attested by the small overlap population value of 0.06. As the rare earth elements have same number of valence electrons and similar orbital energies, the COOP curves are similar for all La, Ce, Pr, Nd and Sm compounds. Therefore, only the COOP curves of the $\text{Ce}_2\text{Pd}_9\text{Sb}_3$ compound are presented here.

The spin-polarized DOS calculated by WIEN2k for $\text{Ce}_2\text{Pd}_9\text{Sb}_3$ is presented in Fig. 5. The upper panel is the DOS of Ce, the middle one Pd and lower one Sb. Since Pd is close to a d^{10} closed shell configuration and Sb^{3-} also in a closed shell state, there is no splitting between the up and down spin states. In contrary, Ce^{3+} has 1 unpaired 4f electron, as a result there is slight splitting of the up and down spin states. The 4f state originally about 0.5 eV above the Fermi level without spin polarization is now around it. The Ce spin up and down states are not symmetric, making it possible contributor to paramagnetism. The calculated magnetic moment inside the rare earth atomic spheres of the La, Ce, Pr, Nd and Sm compounds are 0.00, 0.61, 2.06, 3.15 and 5.45 μ_B , respectively. These values follow the experiment trend of 0.18, 2.23, 3.46, 3.57 and 1.42 μ_B/Ln^{3+} of this series except for the Sm compound (see the next section and Table 4). It is well-known that due to strong spin-orbit coupling, the ground state of Sm^{3+} ion is $^6H_{5/2}$ with a much lower theoretical spin of 0.85 [22, 23]. In the current implementation of LDA or LDA+U, the WIEN2k package failed to correctly calculate the spin of the Sm^{3+} species.

Magnetic properties

According to the susceptibility measurements, the Sm compound is paramagnetic below room temperature exhibiting the Curie-Weiss behavior down to about 10 K. The obtained paramagnetic temperature theta is 1 K suggesting the dominance of small ferromagnetic coupling. Isothermal magnetization measurements reveal a tendency to saturation below this temperature. Plot of the data following the Arrott-Belov [24] method shows that the Curie temperature is slightly below 7 K. A precise analysis can be done by interpolation between the measured isotherms. This gives an estimation of 6.8 K for the hypothetical curves passing at the origin (Fig. 6). At 2 K and a field of 10 T the measured magnetization is only about 0.55 $\mu_B/\text{f.u.}$, a rather small value for ordered Sm state taking into account the presence of two Sm atoms per formula unit. This is partly due to the not fully saturated state of the magnetization curve as can be seen from Fig. 7, thus reflecting a possibly large magnetocrystalline anisotropy. In addition, bearing in mind that the Pd atom is close to the Stoner criterion, one may expect a significantly large magnetic moment induced on the Pd atoms and possibly on the Sb one as well. The analysis of the susceptibility curves from 20 to 300 K leads to an effective magnetic moment of 1.42 μ_B/Sm in comparison with an expected value of

$\mu_{\text{eff.}}(\text{Sm}^{3+}) = 0.85 \mu_{\text{B}}$ for ground state ${}^6H_{5/2}$ configuration against $3.32 \mu_{\text{B}}$ for ${}^6H_{7/2}$ configuration. This is most probably arises from the small spin-orbit coupling in Sm^{3+} enabling mixing of states. Similar investigations have been carried out on the samples with $Ln = \text{Ce}, \text{Pr}$ and Nd . The corresponding data are plotted in Figs. 8-10. Due to a very weak effect, ordering temperatures cannot be properly defined from M/H data. However, tend to magnetic ordering is visible from field dependent magnetization curves (Figs. 8-10). Thus, the temperature and nature of ordering was estimated based on Arrott-Belov plots and taking into account sign of θ_p . Magnetic susceptibility at 1 T and 0.1 T are similar. Plots of the inverse susceptibility (Fig. 11) have curvature, thus a modified Curie-Weiss model was applied to fit this dependence (20-300 K): $M/H = \chi_0 + C/(T-\theta_p)$, where χ_0 – temperature independent magnetic contribution, C – Curie constant, used for extraction of effective magnetic moment ($\mu_{\text{eff.}}$), θ_p – paramagnetic Curie-Weiss temperature. Obtained parameters for $\mu_0H = 1$ T curves are listed in Table 4 and the fitted curves are shown in Fig. 11. The $\text{Pr}_2\text{Pd}_9\text{Sb}_3$ compound exhibits a negative Curie-Weiss temperature $\theta_p = -3.71(3)$ K, the obtained effective magnetic moment $3.46 \mu_{\text{B}}/\text{Pr}$ which is close to the free ion value. The magnetic ordering temperature is estimate to be 6 K for $\text{Pr}_2\text{Pd}_9\text{Sb}_3$. At 2 K the isothermal magnetization curves recoded at 2K is indicative of an ferromagnetic like behaviour. Under a field of 10 T, the magnetization value is $3.2 \mu_{\text{B}}/\text{f.u.}$ taking two Pr atoms per formula unit, one get to $1.6 \mu_{\text{B}}/\text{Pr}$ whereas a value of $3.2 \mu_{\text{B}}/\text{Pr}$ can be expected from the free Pr^{3+} ion value. However, such reduced value is often observed in Pr intermetallic compounds and $1.58 \mu_{\text{B}}$ was reported for PrCo_5 [25]. The origin of such reduction may originate from a mechanism involving $4f$ - $3d$ hybridization, itself favored by $3d$ - $5d$ hybridization as describe elsewhere [26, 27].

The analysis of the $\text{Nd}_2\text{Pd}_9\text{Sb}_3$ compound reveals similar Curie-Weiss behavior of the Pr compound: a small but negative paramagnetic temperature is derived $\theta_p = -6$ K indicating dominance of antiferromagnetic exchange interactions. The effective magnetic moment is $3.57 \mu_{\text{B}}/\text{Nd}$, close to that expected for the free ion value $\mu_{\text{eff.}}(\text{Nd}^{3+}) = 3.62 \mu_{\text{B}}$. The ordering temperature of this compound is estimated to be 2 K from the analysis of the isothermal magnetization curves. The magnetization curves shown in Fig. 9 indicate that the saturation is not reached even at an applied field of 10 T. The maximum value obtained is $3.5 \mu_{\text{B}}/\text{formula unit}$ that is half the value expected for Nd^{3+} . In the antiferromagnetic order scenario, this may reflects that Nd magnetic moments of different sublattices are not fully aligned under such magnetic field.

Unlike the above studied $Ln_2\text{Pd}_9\text{Sb}_3$, the La phase exhibits a paramagnetic behavior down to the lowest temperature used here 2 K. Below room temperature, analysis of the temperature dependence of the magnetic susceptibility of $\text{La}_2\text{Pd}_9\text{Sb}_3$ using the following equation $\chi = \chi_0 + C/(T - \theta_p)$ leads to values of $\chi_0 = -1.3 \cdot 10^{-5} \mu_{\text{B}}/\text{f.u.} \cdot \text{T}$, corresponding to the diamagnetic electronic contribution, probably originating from the inner core electrons. A negative Curie Weiss

temperature $\theta_p = -7$ K and a small paramagnetic effective magnetic moment of $\mu_{\text{eff.}} = 0.36 \mu_B/\text{f.u.}$ are attributed to the overall itinerant electrons mostly from Pd since the La atom has an empty $4f^0$ electronic shell and Sb has full $4d^{10}$ shell.

According to the evolution of the lattice volume versus the lanthanide radius, no anomaly has been observed for the Ce atom indicating that the electronic state of Ce should be trivalent. The isothermal magnetization curve recorded at 20 K exhibits a linear behavior up to 10 T demonstrating the paramagnetic state of the $\text{Ce}_2\text{Pd}_9\text{Sb}_3$ phase. In the paramagnetic state a small negative Weiss temperature of -1 K is derived and an effective moment of $2.23 \mu_B/\text{Ce}$ is calculated. A value similar to that reported earlier for $\text{Ce}_3\text{Ni}_2\text{Ge}_7$ compound but slightly smaller than that reported earlier in reference [3]: 2.51 or the free Ce^{3+} ion value ($2.54 \mu_B$) [28, 29]. The low obtained value for the Weiss temperature is in agreement with that reported previously 2(2)K however of opposite sign the magnitude, both being very close to zero leading to expect a low ordering temperature if any for $\text{Ce}_2\text{Pd}_9\text{Sb}_3$. Isotherm magnetization curves have been recorded down to 2 K as can be seen from Fig. 10: Whereas a pure paramagnetic behavior is observed at 20 and 10 K a progressive curvature of the magnetization curve is noticeable at lower temperature indicating the proximity to an ordered state. Such behavior is even more pronounced at 2 K where a magnetic moment of $2.3 \mu_B$ is measured under an applied field of 10 T. Using Arrott-Belov plots, we conclude that the $\text{Ce}_2\text{Pd}_9\text{Sb}_3$ phase orders magnetically below 4 K a temperature smaller than that investigated earlier in reference [3]. In general, ordering temperatures of $\text{Ln}_2\text{Pd}_9\text{Sb}_3$ are quite low, hence e.g. in Ref [7] T_c for Ce compound was not reached using ^4He -refrigeration down 4.2 K, whereas other parameters are comparable with the present study.

A common feature of the $\text{Ln}_2\text{Pd}_9\text{Sb}_3$ studied here is their remarkably low magnetic ordering temperature. The very low ordering temperature revealed here for the $\text{Ln}_2\text{Pd}_9\text{Sb}_3$ phase is not only due to the localized $4f$ character of the Ln magnetism and the rather weak RKKY interactions but arises also from the dilution of the magnetic lanthanide atoms in the Pd and Sb atoms matrix which are not carrying an intrinsic magnetic moment. Indeed according to the crystal structure investigation described above, the lanthanide are rather far apart with interatomic distances of about 4.2 \AA to the nearest neighbor and 4.8 \AA to the second order neighbor.

Conclusions

No anomaly is observed in the lanthanide dependence of the unit cell volume along the $\text{Ln}_2\text{Pd}_9\text{Sb}_3$ series of compounds. This indicates a trivalent state for all the studied lanthanides ($\text{Ln} = \text{La, Ce, Nd, Pr, and Sm}$). According to the magnetization analysis, the $\text{Ln}_2\text{Pd}_9\text{Sb}_3$ ($\text{Ln} = \text{La, Ce, Nd, Pr, and Sm}$) compounds are exhibiting paramagnetic behavior down to very low temperature (<10 K) and weak

paramagnetic temperature bearing witness to the weakness of the overall magnetic exchange interaction in such crystal structure. The Sm atom exhibits the largest ordering temperature of 6.8 K. The weakness of the ordering temperature and magnetic interactions is attributed to both the low lanthanide concentration and the rather long interatomic distances between magnetic atoms in such crystal structure. At 2 K, the magnetization of these phases is difficult to saturate, even in field of 10 T indicating either large anisotropy or else strong antiferromagnetic interaction between the different magnetic atoms. Further investigation by means of neutron diffraction study would be interesting to determine the precise magnetic structure of the $R_2Pd_9Sb_3$ compounds in the ordered state in particular the orientation of the magnetic moments.

Acknowledgement

V.L. is thankful to French Embassy in Ukraine and University Grenoble Alpes for a financial support to perform part of the work at the Institut Néel CNRS (Grenoble). Authors are gratefully acknowledged to Dr. P. Demchenko (Interfaculty Scientific-Educational Laboratory of X-Ray Structure Analysis, Ivan Franko National University of Lviv, Ukraine) for high quality XRD data collection.

References

- [1] O.L. Sologub, P.S. Salamakha, in: K.A. Gschneidner Jr., J.-C.G. Bünzli, V.K. Pecharsky (Eds.), Handbook on the Physics and Chemistry of Rare Earths, vol. 33, North-Holland, Amsterdam, 2003, pp. 35-146.
- [2] M.V. Zelinska, Synthesis, crystal structure and properties of the ternary pnictides in the Er-{Ni, Pd}-{P, As, Sb} ternary systems and related ones. Thesis for a degree of Candidate of Sciences in Chemistry. Lviv, Lviv University, 2007.
- [3] K. Gofryk, D. Kaczorowski, T. Plackowski, A. Leithe-Jasper, Yu. Grin, Phys. Rev. B. 72 (2005) 094409.
- [4] S. Ganesanpotti, T. Yajima, T. Tohyama, Z. Li, K. Nakano, Y. Nozaki, C. Tassel, Y. Kobayashi, H. Kageyama, J. Alloys Compd. 583 (2014) 151-154.
- [5] Y. Muro, N. Takeda, M. Ishikawa, J. Alloys Compd. 257 (1997) 23-29.
- [6] T. Iwasaki, S. Suga, S. Imada, Y. Kuwata, T. Muro, S. Ueda, M. Saeki, H. Harada, M. Tsunekawa, T. Matsushita, A. Sekiyama, A. Fujimori, H. Ishii, T. Kimura, T. Miyahara, T. Suzuki, K. Katoh, A. Ochiai, J. Electron. Spectrosc. Relat. Phenom. 88-91 (1998) 309-314.
- [7] R.A. Gordon, F.J. DiSalvo, R. Pöttgen, N.E. Brese, J. Chem. Soc. 92 (1996) 2167-2171.
- [8] O. Zhak, A. Fedyna, I. Hladka, Visnyk Lviv Univ. Series Chemistry. 57(1) (2016) 112-121.
- [9] L. Akselrud, Yu. Grin, J. Appl. Crystallogr. 47 (2014) 803-805.
- [10] R. Hoffmann, Chem. Phys. 39 (1963) 1397-1412.
- [11] M.H. Whangbo, R. Hoffmann, R.B. Woodward, Proc. R. Soc. London, A366 (1979) 23.
- [12] P. Blaha, K. Schwarz, G.K.H. Madsen, D. Kvasnicka, J. Luitz, R. Laskowski, F. Tran, L.D. Marks, WIEN2k, An Augmented Plane Wave + Local Orbitals Program for Calculating Crystal Properties (Karlheinz Schwarz, Techn. Universitat Wien, Austria), 2018. ISBN 3-9501031-1-2.
- [13] A. Barlet, J.C. Genna, P. Lethuillier, Cryogenics 31 (1991) 801-805.
- [14] Yu. Grin, R.E. Gladyshevskii, O.M. Sichevych, V.E. Zavodnik, Ya.P. Yarmolyuk, I.V. Rozhdestvenskaya, Sov. Phys. Crystallogr. 29 (1984) 528-530.
- [15] F.C. Frank, J.S. Kasper, Acta Crystallogr. 11 (1958) 184-190.
- [16] Wiberg N. Lehrbuch der Anorganischen Chemie, Walter de Gruyter, Berlin, 1995, pp. 1838-1841.
- [17] R.A. Gordon, F.J. DiSalvo, R. Pöttgen, J. Alloys Compd. 228 (1995) 16-22.

- [18] R.A. Gordon, F.J. DiSalvo, Z. Naturforsch. 51b (1996) 52-56.
- [19] W.K. Hofmann, W. Jeitschko, Monatsh. Chem. 116 (1985) 569-580.
- [20] R.D. Shannon, J. Acta. Crystallogr. A32 (1976) 751-766.
- [21] K.M. Merz Jr., R. Hoffmann, Inorg. Chem. 27 (1988) 2120-2127.
- [22] R. J. Elliott, [Magnetic Properties of Rare Earth Metals, Springer-Verlag, Boston, 1972.](#)
- [23] J. Jensen, A. R. Mackintosh, [Rare Earth Magnetism: Structures and Excitations, Clarendon Press, Oxford, 1991.](#)
- [24] A. Arrott, Phys. Rev. B 108 (1957) 1394-1396.
- [25] E. Burzo, A. Chelkowski, H.R. Kirchmayr, Numerical Data and Functional Relationships in Science and Tehnology New series, Group III, vol. 19, subvolume d2, Landolt-Börnstein, Springer-Verlag, Berlin, 1990.
- [26] N. Coroian, V. Klosek, O. Isnard, J. Alloys Compd. 427 (2007) 5-10.
- [27] D. Givord, D. Courtois, J. Magn. Magn. Mater. 196-197 (1999) 684-688.
- [28] L. Durivault, F. Bourrée, B. Chevalier, G. André, J. Etourneau, O. Isnard, J. Magn. Magn. Mater. 232 (2001) 139-146.
- [29] S. Matar, B. Chevalier, O. Isnard, J. Etourneau, J. Mater. Chem. 13 (2003) 916-920.

Table 1. Crystal data and structure refinement details for the $Ln_2Pd_9Sb_3$ compounds ($Ln = La, Ce, Pr, Nd, Sm$)

Compound	$La_2Pd_9Sb_3$ [4]	$Ce_2Pd_9Sb_3$	$Pr_2Pd_9Sb_3$	$Nd_2Pd_9Sb_3$	$Sm_2Pd_9Sb_3$
Structure type	Ce ₂ Pd ₉ Sb ₃ (anti- Y ₂ Co ₃ Ga ₉)				
Space group	<i>Cmcm</i>				
Number of formula units	<i>Z</i> = 4				
Lattice parameters: <i>a</i> , Å	13.7772(6)	13.7417(7)	13.7392(6)	13.7208(5)	13.6957(7)
<i>b</i> , Å	8.0642(3)	8.0328(4)	8.0146(3)	7.9983(3)	7.9686(4)
<i>c</i> , Å	9.3967(4)	9.3394(5)	9.3215(4)	9.3016(3)	9.2700(5)
<i>V</i> , Å ³	1044.0(1)	1030.9(2)	1026.4(1)	1020.8(1)	1011.7(2)
Calculated density, g/cm ³	10.183(1)	10.328(2)	10.386(1)	10.484(1)	10.658(2)
Absorption coefficient	2444.88	2541.71	2576.48	2627.17	2726.13
Diffractometer	STOE STADI P				
Radiation and wavelength	CuK _{α1} , λ = 1.54056 Å				
Number of atoms in cell / positions	56 / 7				
Number of free parameters	20				
2θ _{max} i (sinθ/λ) _{max}	110, 0.534				
Final R-values: <i>R</i> _i	0.0449	0.0550	0.0470	0.0442	0.0485
<i>R</i> _P	0.0397	0.0430	0.0400	0.0313	0.0289
<i>wR</i> _P	0.0577	0.0619	0.0584	0.0449	0.0431

Table 2. Atomic positional and displacement parameters for the crystal structure of $Ln_2Pd_9Sb_3$ compounds ($Ln = La, Ce, Pr, Nd, Sm$) as derived from room temperature X-ray powder diffraction investigation

Atoms	Wyckoff site	x/a	y/b	z/c	$B_{iso}, \text{\AA}^2$
La₂Pd₉Sb₃ [4]					
La	8g	0.3446(3)	0.3258(6)	1/4	1.13(6)
Pd1	16h	0.1700(2)	0.1706(5)	0.0817(2)	1.14(6)
Pd2	8g	0.0994(3)	0.4587(5)	1/4	1.56(10)
Pd3	8f	0	0.3327(7)	0.5264(3)	0.79(8)
Pd4	4c	0	0.1433(7)	1/4	0.51(13)
Sb1	8e	0.3248(2)	0	0	1.16(7)
Sb2	4a	0	0	0	1.03(13)
Ce₂Pd₉Sb₃					
Ce	8g	0.3438(5)	0.3250(9)	1/4	0.53(9)
Pd1	16h	0.1698(4)	0.1720(8)	0.0853(4)	0.63(9)
Pd2	8g	0.0988(5)	0.4610(8)	1/4	0.68(13)
Pd3	8f	0	0.3356(11)	0.5244(6)	0.4(3)
Pd4	4c	0	0.1473(12)	1/4	0.70(15)
Sb1	8e	0.3223(4)	0	0	0.4(2)
Sb2	4a	0	0	0	0.51(13)
Pr₂Pd₉Sb₃					
Pr	8g	0.3413(3)	0.3292(7)	1/4	1.08(7)
Pd1	16h	0.1707(3)	0.1700(6)	0.0832(3)	0.52(6)
Pd2	8g	0.0988(3)	0.4591(6)	1/4	1.24(11)
Pd3	8f	0	0.3329(8)	0.5309(4)	0.49(9)
Pd4	4c	0	0.1503(9)	1/4	0.9(2)
Sb1	8e	0.3248(3)	0	0	0.60(7)
Sb2	4a	0	0	0	0.4(1)
Nd₂Pd₉Sb₃					
Nd	8g	0.3455(3)	0.3264(6)	1/4	1.23(6)
Pd1	16h	0.1720(3)	0.1712(5)	0.0854(3)	1.17(6)
Pd2	8g	0.0984(3)	0.4627(5)	1/4	1.57(9)
Pd3	8f	0	0.3301(7)	0.5300(4)	1.34(8)
Pd4	4c	0	0.1466(8)	1/4	1.10(4)
Sb1	8e	0.3236(2)	0	0	1.36(9)
Sb2	4a	0	0	0	1.2(2)
Sm₂Pd₉Sb₃					
Sm	8g	0.3459(3)	0.3276(9)	1/4	0.49(9)
Pd1	16h	0.1713(3)	0.1705(8)	0.0865(3)	1.06(9)
Pd2	8g	0.0972(4)	0.4600(7)	1/4	1.2(2)
Pd3	8f	0	0.3311(9)	0.5341(4)	0.60(9)
Pd4	4c	0	0.1463(9)	1/4	1.2(2)
Sb1	8e	0.3248(2)	0	0	1.16(7)
Sb2	4a	0	0	0	1.0(1)

Table 3. Interatomic distances δ and coordination numbers (CN) of the atoms in the $\text{Nd}_2\text{Pd}_9\text{Sb}_3$ structure

Atom	δ , Å	CN	Atom	δ , Å	CN	
$\text{Nd}_2\text{Pd}_9\text{Sb}_3$						
Nd – 1Pd2	3.010(6)	17	Pd3 – 1Sb2	2.655(6)	13	
2Pd1	3.091(5)		1Pd3	2.775(8)		
2Pd1	3.129(2)		2Sb1	2.790(4)		
2Pd1	3.163(5)		2Pd1	2.887(4)		
2Pd3	3.201(4)		2Pd2	2.959(5)		
1Pd4	3.324(6)		1Pd4	2.990(5)		
2Sb2	3.439(3)		2Pd2	3.120(4)		
2Sb1	3.509(3)		2Nd	3.201(4)		
1Pd2	3.561(5)					
2Sb1	3.566(4)					
			Pd4 – 2Sb2	2.604(3)		12
			4Pd1	2.819(3)		
			2Pd2	2.866(7)		
			2Pd3	2.990(5)		
			2Nd	3.324(6)		
Pd1 – 1Sb1	2.614(4)	12	Sb1 – 2Pd2	2.577(2)	12	
1Sb1	2.748(4)		2Pd1	2.614(4)		
1Pd4	2.819(3)		2Pd1	2.748(4)		
1Sb2	2.841(3)		2Pd3	2.790(4)		
1Pd3	2.887(4)		2Nd	3.509(3)		
1Pd1	2.950(5)		2Nd	3.566(4)		
1Pd2	2.966(5)					
1Pd1	3.062(3)					
1Nd	3.091(5)					
1Nd	3.129(2)					
1Nd	3.163(5)					
1Nd	3.166(5)					
			Sb2 – 2Pd4	2.604(3)	12	
			2Pd3	2.655(6)		
			4Pd1	2.841(3)		
			4Nd	3.439(3)		
Pd2 – 2Sb1	2.577(2)	12				
1Pd2	2.700(5)					
1Pd4	2.866(7)					
2Pd3	2.959(5)					
2Pd1	2.966(5)					
1Nd	3.010(6)					
2Pd3	3.120(4)					
1Nd	3.561(5)					

Table 4. Magnetic parameters of the $Ln_2Pd_9Sb_3$ samples ($Ln = La, Ce, Pr, Nd, Sm$)

$Ln_2Pd_9Sb_3$	χ_0 ($\mu_B/f.u. \cdot T$)	C ($K \cdot \mu_B/f.u. \cdot T$)	θ_p (K)	μ_{eff}	M at 2 K and 10 T	T_c (K)
$La_2Pd_9Sb_3$	$-1.3(7) \cdot 10^{-5}$	0.03(1)	-7(2)	0.36 ($\mu_B/f.u.$)	–	–
$Ce_2Pd_9Sb_3$	$1.17(6) \cdot 10^{-2}$	2.23(2)	-1.1(3)	2.39 (μ_B/Ce)	2.3 $\mu_B/f.u.$	4
$Pr_2Pd_9Sb_3$	$6.9(6) \cdot 10^{-3}$	5.37(2)	-3.71(3)	3.46 (μ_B/Pr)	3.2 $\mu_B/f.u.$	6.2
$Nd_2Pd_9Sb_3$	$1.0(3) \cdot 10^{-3}$	5.71(2)	-6.2(2)	3.57 (μ_B/Nd)	3.5 $\mu_B/f.u.$	2
$Sm_2Pd_9Sb_3$	$2.9(1) \cdot 10^{-3}$	0.90(2)	1.0(2)	1.42 (μ_B/Sm)	0.55 $\mu_B/f.u.$	6.8

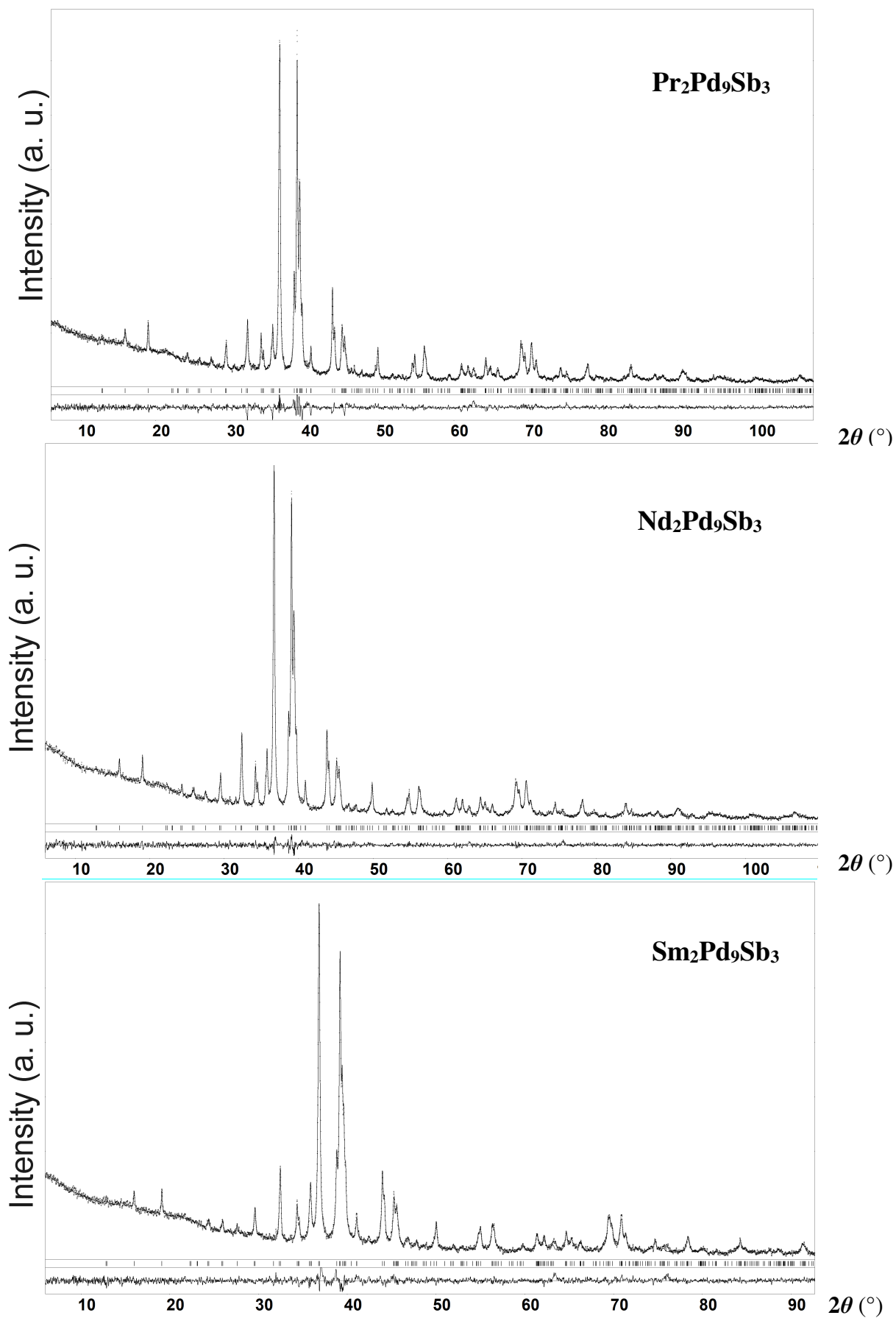


Fig. 1. Observed (dots), calculated (line) and difference (bottom line) XRD profiles for $Ln_2\text{Pd}_9\text{Sb}_3$ samples ($Ln = \text{Pr}, \text{Nd}, \text{Sm}$).

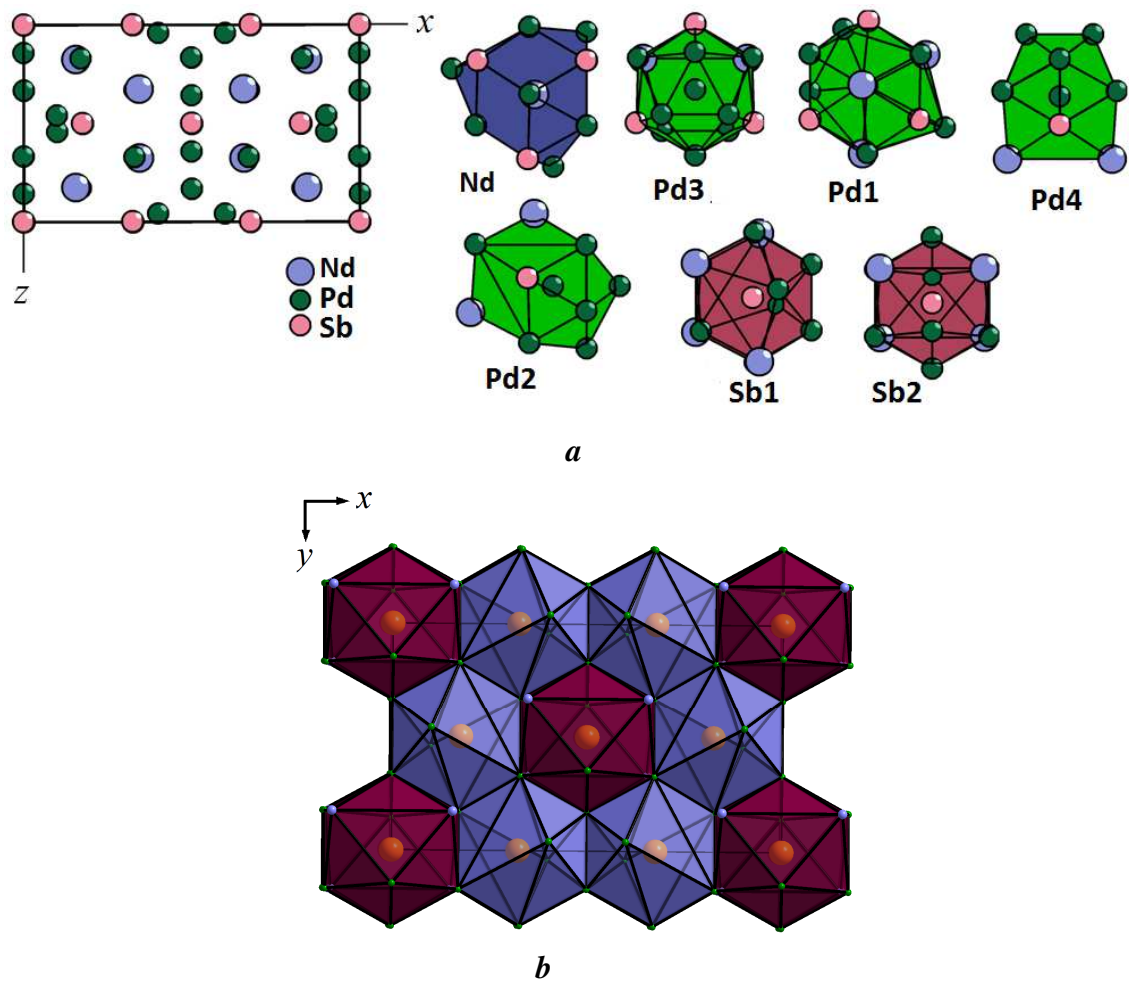


Fig. 2. (a) – Crystal structure of the $\text{Nd}_2\text{Pd}_9\text{Sb}_3$ antimonide ($\text{Ce}_2\text{Pd}_9\text{Sb}_3$ type), coordination polyhedra of atoms; (b) – arrangement of Sb1 (blue) and Sb2 (red) polyhedra in the structure, the size of the atoms Pd and Nd is reduced for better perception.

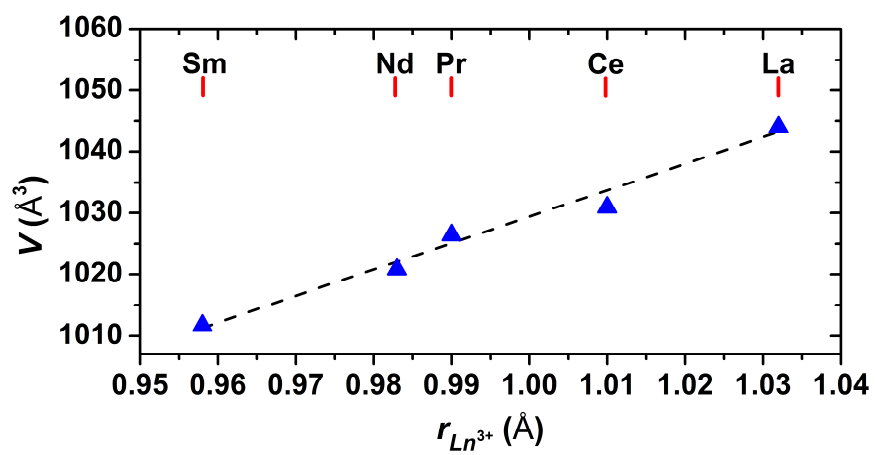


Fig. 3. Dependence of the unit cell volumes, V , on the values of the Ln^{3+} radii

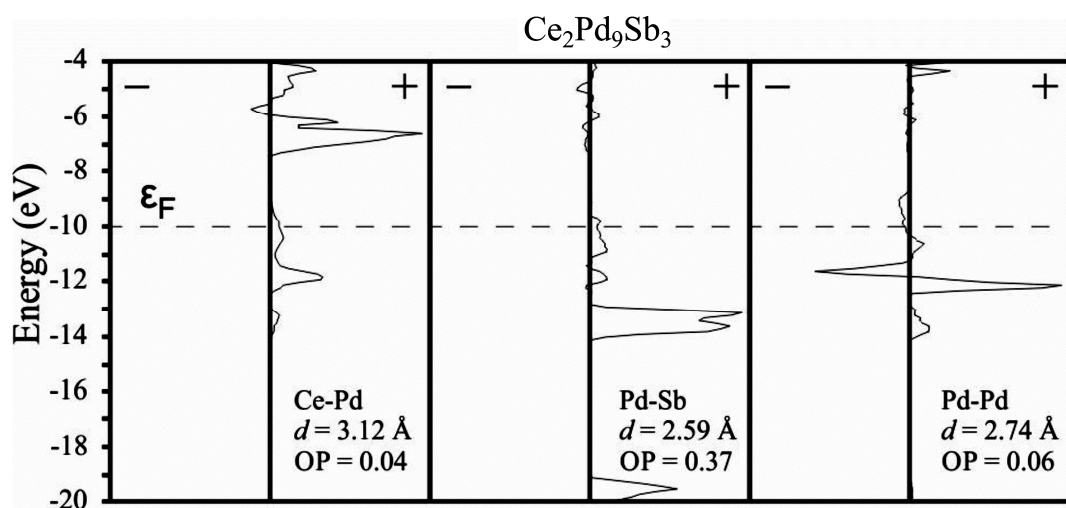


Fig. 4. EH *COOP* curves of representative bonds in $\text{Ce}_2\text{Pd}_9\text{Sb}_3$. The + region is the bonding area and the - region the antibonding area. The bond type, distance and integrated overlap population up to the Fermi level are indicated in each panel.

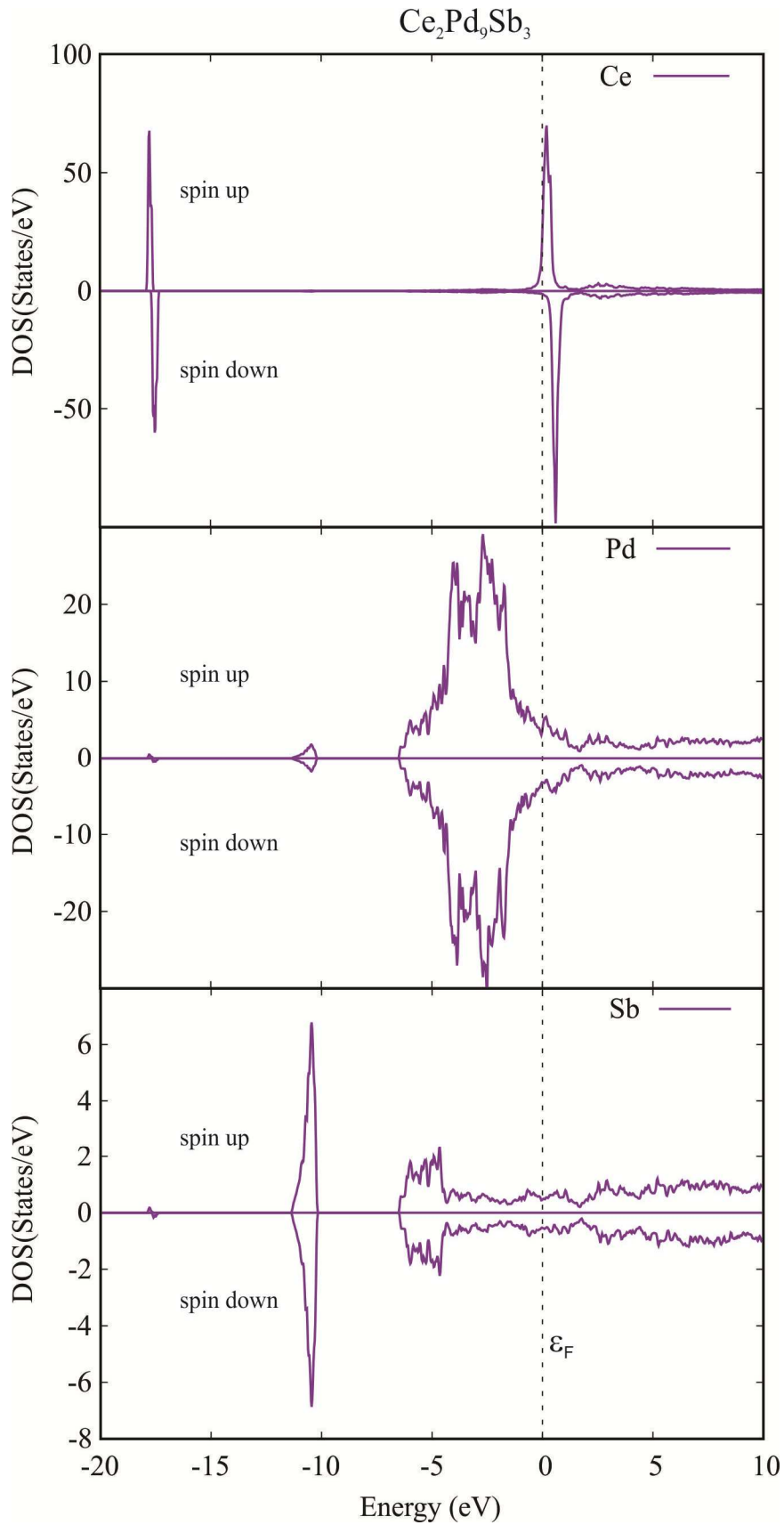


Fig. 5. Spin-polarized DOS of $\text{Sm}_2\text{Pd}_9\text{Sb}_3$ calculated by the WIEN2k package. The upper panel is the total DOS of Sm, most of it is Ce 4*f* near the Fermi level. The middle one is the total DOS of Pd, most of it is the 4*d* of Pd. The lower panel is the total DOS of Sb.

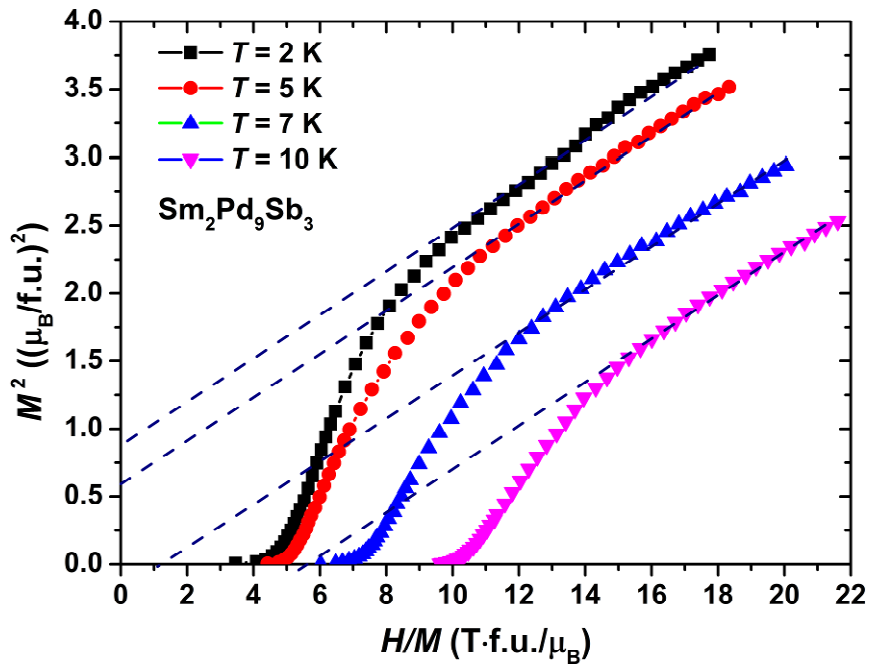


Fig. 6. Arrott-Belov plots for $\text{Sm}_2\text{Pd}_9\text{Sb}_3$, at the indicated temperature.

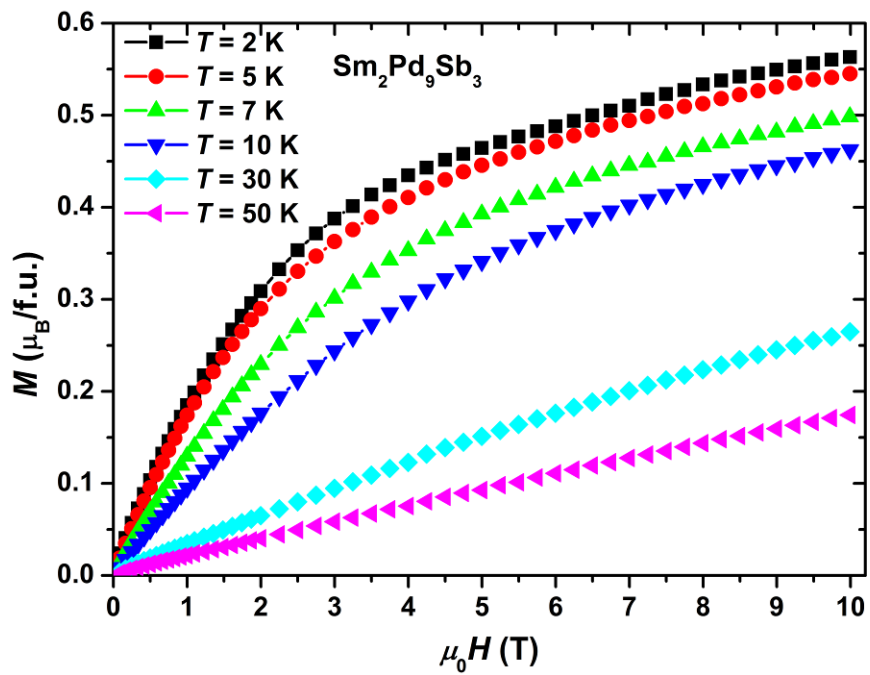


Fig. 7. Isothermal magnetization curves of $\text{Sm}_2\text{Pd}_9\text{Sb}_3$ recorded at the indicated temperature.

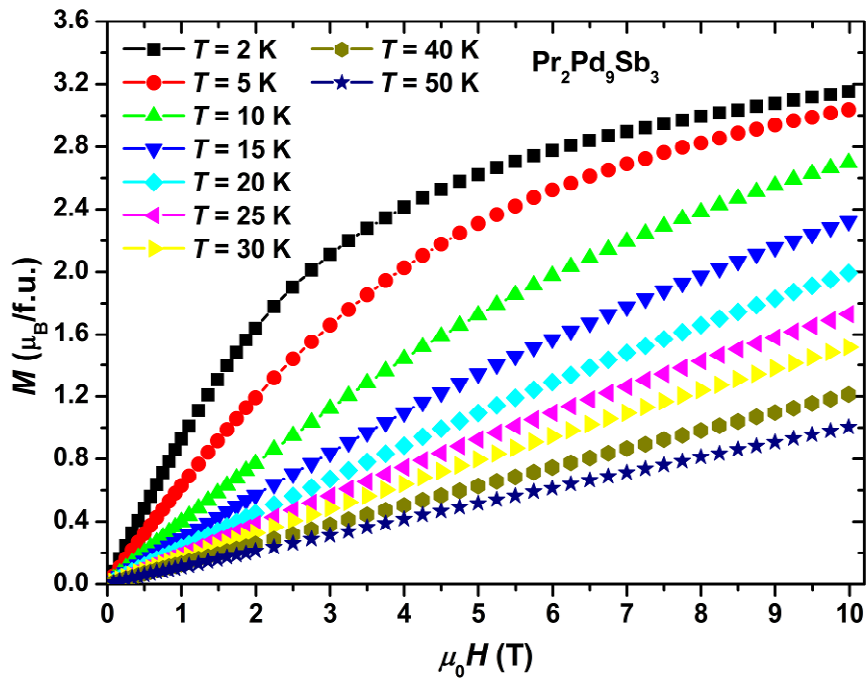


Fig. 8. Isothermal magnetization curves of $\text{Pr}_2\text{Pd}_9\text{Sb}_3$ recorded at the indicated temperature.

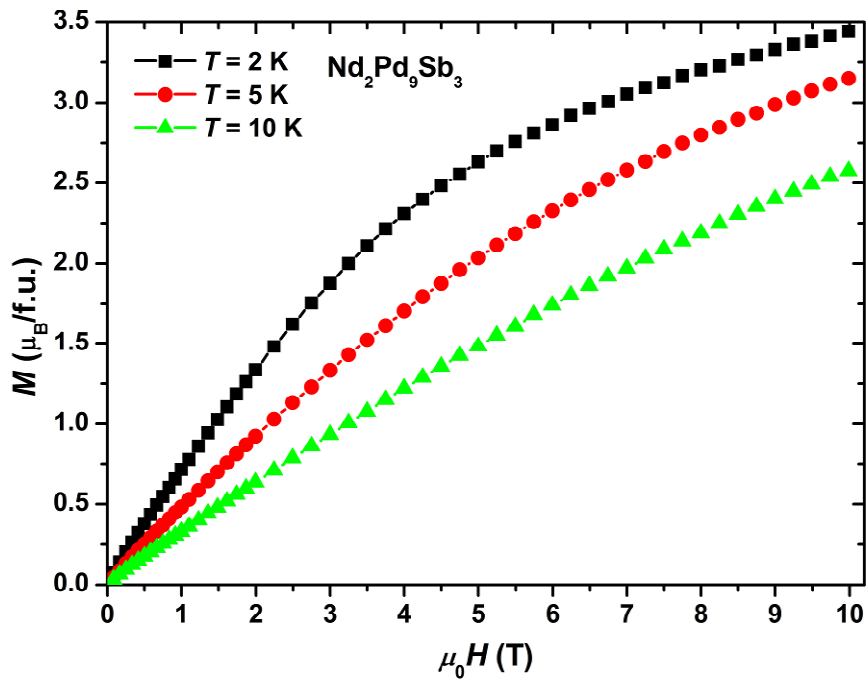


Fig. 9. Isothermal magnetization curves of $\text{Nd}_2\text{Pd}_9\text{Sb}_3$ recorded at the indicated temperature.

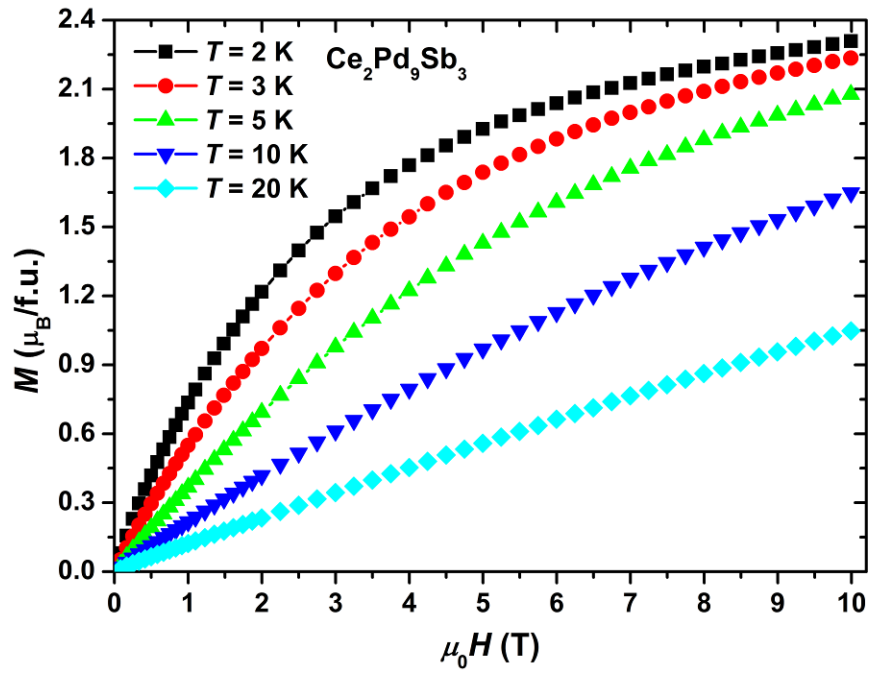


Fig. 10. Isothermal magnetization curves of $\text{Ce}_2\text{Pd}_9\text{Sb}_3$ recorded at the indicated temperature.

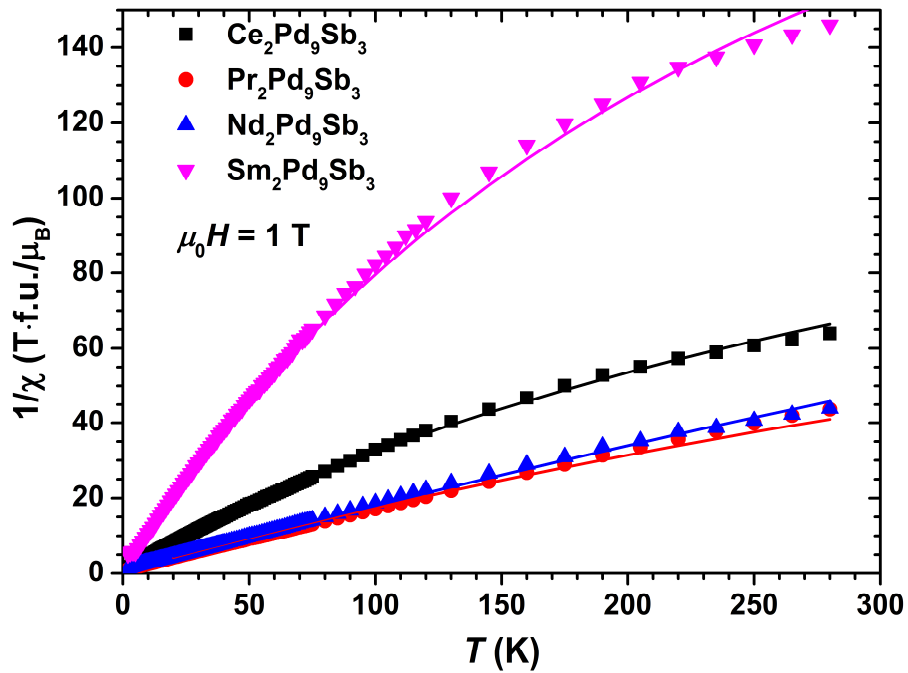


Fig. 11. Reciprocal susceptibility vs temperature for $\text{Ln}_2\text{Pd}_9\text{Sb}_3$ ($\text{Ln} = \text{Ce}, \text{Pr}, \text{Nd}, \text{Sm}$) samples in a magnetic field $\mu_0 H = 1 \text{ T}$ (solid lines – modified Curie-Weiss fit)

